

# Influence of sea-land breeze on the formation and dissipation of severe dense fog and its burst reinforcement in the Yellow Sea coastal area, China

Ya GAO<sup>1,2</sup>, Duanyang LIU<sup>1,3,4\*</sup>, Shuqi YAN<sup>1,3,4</sup>, Wenjun ZHOU<sup>1,2</sup>, Hongbin WANG<sup>1,3</sup>, Fan ZU<sup>1,3</sup>, Qin MEI<sup>2</sup>, Chuanxiang YI<sup>2</sup> & Ye SHENG<sup>2</sup>

<sup>1</sup> Key Laboratory of Transportation Meteorology of China Meteorological Administration, Nanjing 210041, China;

<sup>2</sup> Yancheng Meteorological Bureau, Yancheng 224000, China;

<sup>3</sup> Nanjing Joint Institute for Atmospheric Sciences, Nanjing 210041, China;

<sup>4</sup> Key Laboratory of Disaster Weather, Chinese Academy of Meteorological Sciences, Beijing 100086, China

Received August 17, 2022; revised August 24, 2023; accepted December 15, 2023; published online December 29, 2023

**Abstract** Based on the global reanalysis data of the National Centers for Environmental Prediction (NCEP)/National Center for Atmospheric Research, the surface meteorological observation data, sounding data and satellite observation data, this paper comprehensively analyzes the evolution process and formation mechanism of a persistent severe dense fog process occurred on February 15–17, 2015 in Yancheng, eastern China. Through the numerical simulation experiment of Weather Research and Forecast (WRF) model, we further analyze the impact of sea-land breeze on the formation and burst reinforcement of fog. Results show that the precipitation caused by the southwesterly airflow in front of the upper-level trough and the low-pressure inverted trough are conducive to the formation of early rain fog, while the nighttime clear radiance under the control of surface cold high and the infiltration of weak cold advection are conducive to the formation and development of later radiation-advection fog. The WRF model simulates the fog evolution process, which is basically consistent with the actual fog area, and the simulation results are credible to a certain extent. The simulation results show that the establishment of sea breeze has an advection cooling effect on the near surface layer, which is conducive to the formation and development of the inversion layer on the near surface, providing stable stratification conditions for the formation and burst reinforcement of fog. On one hand, the strengthening of sea breeze circulation can continuously transport water vapor to the study area. On the other, the occurrence of ultra-low level jet is favorable for the accumulation of low-level water vapor. At the same time, the inversion intensity further strengthens, which is in favor of the burst reinforcement and long-term maintenance of fog.

**Keywords** Radiation-advection fog, Sea-land breeze, Atmospheric boundary layer, Fog burst reinforcement, WRF model

**Citation:** Gao Y, Liu D, Yan S, Zhou W, Wang H, Zu F, Mei Q, Yi C, Sheng Y. 2024. Influence of sea-land breeze on the formation and dissipation of severe dense fog and its burst reinforcement in the Yellow Sea coastal area, China. *Science China Earth Sciences*, 67(2): 432–449, <https://doi.org/10.1007/s11430-022-1243-8>

## 1. Introduction

Fog is a weather phenomenon caused by a large number of water drops or ice crystals suspended in the near-surface atmospheric boundary layer, which can reduce the horizontal

visibility to below 1000 m. Currently, the fog with visibility greater than or equal to 50 m but less than 200 m is classified as severe dense fog, while the fog with visibility less than 50 m is classified as extremely severe dense fog (Compilation of Chinese National Standards: Grade of fog forecast, 2012). Due to the low visibility, fog not only affects the transportation safety, but also leads to poor air quality and

\* Corresponding author (email: [liuduanyang@cma.cn](mailto:liuduanyang@cma.cn))

respiratory illness (Xu et al., 2002). Meanwhile, it is accompanied by such phenomena as fog water acidification (Zhou, 1994). Therefore, as a type of disastrous weather, fog has received more and more attention recently (Bendix et al., 2011; Mu and Zhang, 2014). Based on the differences between fog-haze (Willett, 1928; Taylor, 2007; Wu, 2008; Yin et al., 2015; Liu et al., 2021) and stratiform clouds (Pilié et al., 1923; Okita, 1962; Goodman, 1977), meteorologists at home and abroad utilized observation methods such as the tethered airship (Fuzzi et al., 1992, 1998), meteorological tower (Wu et al., 2008; Wang et al., 2020; Yang et al., 2021), meteorological satellite (Fu et al., 2008; Wang et al., 2018) and rotor drone (Wang et al., 2020) to observe and identify fog and conduct classification research. Many remarkable results have been achieved in the aspects such as atmospheric boundary layer characteristics (Roach et al., 1976; Zhang et al., 2005; Haeffelin et al., 2010; Liu et al., 2011, 2016) and microphysical structures of fog (Meyer et al., 1980; Brenquier et al., 2000; Niu et al., 2010; Liu et al., 2017; Wang et al., 2021; Chen et al., 2021).

In recent years, many scholars have found that the burst reinforcement of severe dense fog occurred frequently, and the fog rapidly enhanced to severe dense fog or extremely severe dense fog in a short period (around 30 min) (Korb and Zdunkowski, 1970). Gultepe et al. (2007) emphasized that the extremely low visibility caused by dense or severe dense fog may seriously affect the safety and efficiency of aviation, maritime and land transportations, and the daily lives of the people, and the economic losses caused by it may be comparable to those caused by tornadoes, even winter storms or hurricanes. According to reports, on December 28, 2022, more than 200 vehicles collided in a pileup at the Zhengzhou-Xinxiang Yellow River Bridge in Zhengzhou, Henan Province of China; on January 8, 2023, a semi-trailer truck collided with pedestrians in Nanchang, Jiangxi Province of China, resulting in 19 deaths and 20 injuries. These traffic accidents were closely related to the burst reinforcement of fog. Therefore, the study on the burst reinforcement characteristics of fog has important practical significance.

Nowadays, it has been nearly fifty years since Korb and Zdunkowski (1970) first proposed the burst reinforcement mechanism, and many research achievements on the fog burst reinforcement have also been obtained at home and abroad. Fuzzi et al. (1992) proposed that the burst reinforcement of fog is related to the advection of fog layer. Price (2011) pointed out that the distributions of stratification and fog droplet size spectrum are important factors leading to sudden variations in the visibility of radiation fog. While observing the atmospheric boundary layer and fog droplet spectrum characteristics of the burst severe dense fog, Li et al. (1999, 2011, 2019) emphasized that the multi-layer inversion temperature structure, latent heat release, surface warming and turbulence mixing play an important role in the

burst development of radiation fog. The increase of supersaturation and the enhancement of turbulent diffusion are also main factors affecting the rapid broadening of fog droplet spectrum. Pu et al. (2008a) found that at night, the enhanced long-wave radiation, near-surface cold advection, surface water evaporation or southwesterly moist advection, and turbulent mixing all can lead to the burst reinforcement of fog. Lu et al. (2010), Liu et al. (2010, 2012) and Niu et al. (2012) analyzed the burst reinforcement of fog in Nanjing, and found that during the burst reinforcement stage, there are many microphysical characteristics such as the uplifting and broadening of fog droplet spectrum, and the rapid increase of water content and average diameter. Wu et al. (2014) pointed out that the infiltration of weak cold air in the leading edge of front is the direct reason for the local burst reinforcement of radiation fog. Jiao et al. (2016) proposed that the invasion of weak cold air is a promoting factor for the burst reinforcement of fog in Jiangsu. Yan et al. (2018) analyzed a case of large-scale burst severe dense fog, and indicated that the long-wave radiation cooling, rainfall before the fog and low-level jet are important reasons for the fog formation and burst development. Liang et al. (2019) found that the strong near-surface temperature inversion layer is also a key factor leading to the burst reinforcement of fog. Although significant progress has been achieved in the study of burst severe dense fog, whether there are certain regional differences in the characteristics and causes of fog burst in different regions is still worth further research.

Yancheng is a city of Jiangsu Province in China, and is located in the coastal area of the Yellow Sea. Affected by the geographical location and the subtropical monsoon climate, the fog process occurs frequently in Yancheng in autumn and winter. Especially, the regional severe dense fog process brings huge losses and inconveniences to local productions and lives, and leads to adverse effects on traffics. The uncertainty of fog influencing factors also increases the difficulty in fog forecast and warning signal issuing. A persistent severe dense fog process occurred on February 15–17, 2015 in Yancheng, which has a long duration and strong intensity, causing huge impact far exceeding that of general fog weather.

Based on the global reanalysis data of the National Centers for Environmental Prediction/National Center for Atmospheric Research, the conventional observation data, sounding data and satellite observation data, this study analyzes the evolution process, synoptic situation and formation mechanism of this severe dense fog process. Furthermore, the circulation background and meteorological element characteristics are investigated. Then, the causes of fog burst reinforcement during the period of severe dense fog are analyzed in detail. It is worth noting that previous studies on the factors affecting the burst reinforcement of fog mostly focused on such aspects as the radiation cooling, inversion

layer, cold and warm advections and turbulence, while the influence of sea-land breeze on fog was mostly mentioned in the observation and numerical simulation of sea fog. For example, Choi and Speer (2006) found that the overlying of sea breeze and easterly near-shore breeze can easily reduce the regional wind speed and lead to water vapor saturation and condensation, and then the coastal advection fog is formed under the effect of radiation cooling. Wang et al. (2012) presented that the formation and dissipation of sea fog correspond well with the transition between northerly wind and southerly wind. Jin et al. (2022) pointed out that the sea fog formation is positively correlated with the land breeze circulation and negatively correlated with the sea breeze circulation. For the coastal fog, the sea-land interaction is more complex.

In the severe dense fog case of this study, it is found that the occurrence of sea-land breeze also has a certain impact on the burst reinforcement of fog. Through the numerical simulation experiment of Weather Research and Forecast (WRF) model, we further analyze the impact of sea-land breeze on the formation and development of fog in terms of thermodynamics, dynamics and water vapor. We hope the results of this study can provide some reference for improving the now-casting and early warning of local severe dense fog.

## 2. Study area, observation data and method

### 2.1 Study area

In the four near-shore sea areas in China, fog occurs most frequently in the Yellow Sea area (Wang, 1980). Therefore, we select Yancheng City as the study area, which faces the Yellow Sea in the east (Figure 1). Wei et al. (2010) pointed out that the number of fog days in the coastal areas of Jiangsu shows a decrease order of the Jianghuai region, the southern Jiangsu region and the Huabei region. Wang et al. (2021) found that the large values of fog hours in Jiangsu from 2013 to 2018 distribute along the Yangtze River and Huai River, as well as in the areas north of them, and the severe dense fog and extremely severe dense fog concentrate along the Huai River and the areas north of it. Yancheng City crosses over the Jianghuai and Huabei regions. According to the observation data, fog processes frequently occur in Yancheng. Because it is located in the middle latitudes and in the transition zone from the subtropical zone to the warm temperate zone, the sea-land temperature difference is significant, and thus the coastal areas of the Yellow Sea are often affected by sea-land breeze (Wang and Song, 1989).

### 2.2 Observation data and model scheme

The data used in this study are observation data from 8 basic

meteorological stations, including Yancheng (YC), Xiangshui (XS), Binhai (BH), Funing (FN), Jianhu (JH), Sheyang (SY), Dongtai (DT), Dafeng (DF), and 29 regional meteorological stations on February 15–17, 2015 (including visibility, air temperature, wind direction, wind speed, relative humidity, precipitation, etc, the temporal resolutions of visibility and precipitation are 10 minutes, while the temporal resolutions of wind, temperature, humidity, and pressure are 5 minutes), the global reanalysis data ( $2.5^{\circ} \times 2.5^{\circ}$ ) and final operational global analysis data ( $1^{\circ} \times 1^{\circ}$ ) of the National Centers for Environmental Prediction/National Center for Atmospheric Research (temporal resolution: 6 hours), the L-band radar sounding observation data at Sheyang station ( $33.46^{\circ}\text{N}, 120.15^{\circ}\text{E}$ ) at 08:00 (Beijing Time, the same below) and 20:00 BJT (including temperature, humidity, wind direction, wind speed at different altitudes) and the black-body brightness temperature observation data (temporal resolution: 1 hours) of Multi functional Transport Satellite geostationary meteorological satellite in Japan.

The WRF (V3.9.1.1), which is a new generation of mesoscale numerical weather prediction model, is used in this study. Currently, this model has been used in a large amount of work to simulate fog processes and explore the mechanisms (van der Velde et al., 2010; Lu et al., 2014; Jia and Guo, 2015; Ding et al., 2019; Yan et al., 2020; Yan et al., 2021). The simulation is configured with two static and two-way nested domains, and the center of the simulation domain is at  $119.5^{\circ}\text{E}, 33.0^{\circ}\text{N}$  (Figure 2). There are both  $109 \times 109$  grid points in the outer-domain and inner-domain, and the grid intervals are 15 km and 5 km, respectively. The inner domain covers the range of this fog process.

The boundary layer parameterization scheme selects the Yonsei University scheme (Hong et al., 2006), and the microphysical scheme adopts the Lin dual-parameter scheme (Lin et al., 1983). Other physical parameterization schemes are described in Table 1. In order to describe the boundary layer process, the vertical grids are added into 42 layers, with 9 layers below 100 m and the lowest level at 8 m. The dense vertical levels can favor the simulation effect of fog (Yan et al., 2021). The meteorological driving field uses the ERA5 Interim reanalysis data with a resolution of  $0.25^{\circ} \times 0.25^{\circ}$ . The model integrates for 78 hours from 08:00 BJT on February 14 to 14:00 BJT on February 17, 2015. The first 24 hours are the spin up time. In the simulation, if the liquid water content is larger than  $0.015 \text{ g kg}^{-1}$  within the boundary layer, then we deem there is fog, and correspondingly the visibility in the fog is less than 1 km (Kunkel, 1984).

### 2.3 Identification of dense fog

The identification of fog in this study is based on the visibility and relative humidity observation data at meteorological stations. The thresholds of visibility and relative

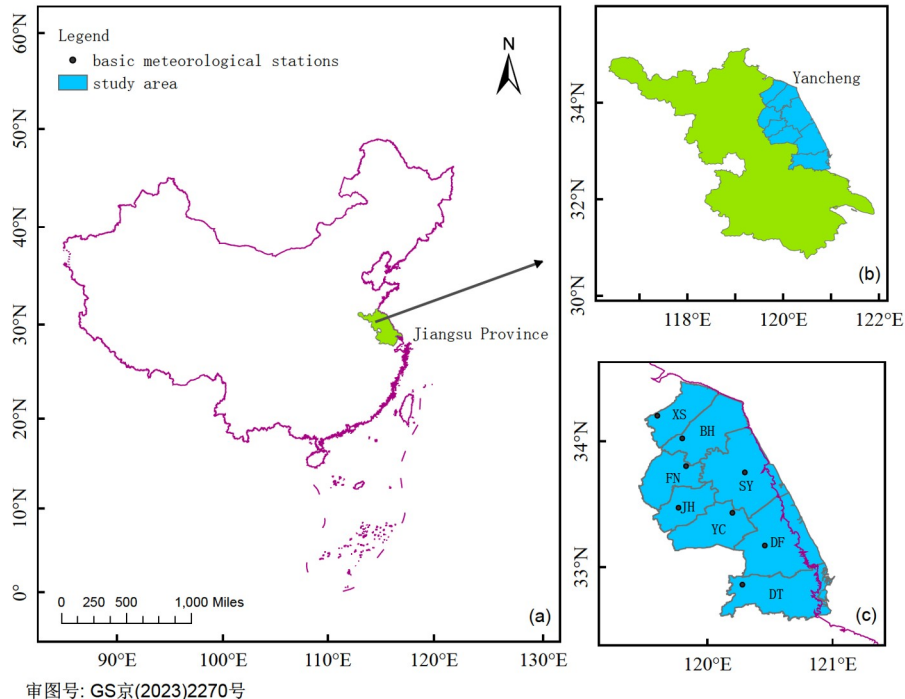


**Figure 1** (a) Geographical location of Jiangsu Province; (b) the study area of this paper: Yancheng; (c) 8 meteorological stations in the study area (Xiangshui: XS; Binhai: BH; Funing: FN; Jianhu: JH; Sheyang: SY; Yancheng: YC; Dafeng: DF; Dongtai: DT), the same below. The black solid line in Figure 1c is the coastline, and the color area on the right side of the coastline is mudflat.

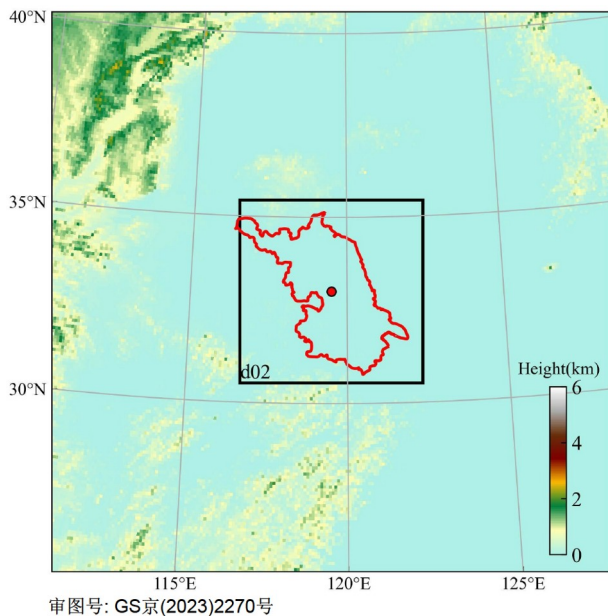


**Figure 2** The simulation domain of the WRF model.

humidity are 1 km and 90%, respectively (Guo et al., 2015; Ma et al., 2014). According to the Grade of fog forecast (GB/T 27964-2011) of the Compilation of Chinese National Standards (2012), the fog with visibility greater than or equal to 200 m but less than 500 m is classified as dense fog, the fog with visibility greater than or equal to 50 m but less than 200 m is classified as severe dense fog, and the fog with

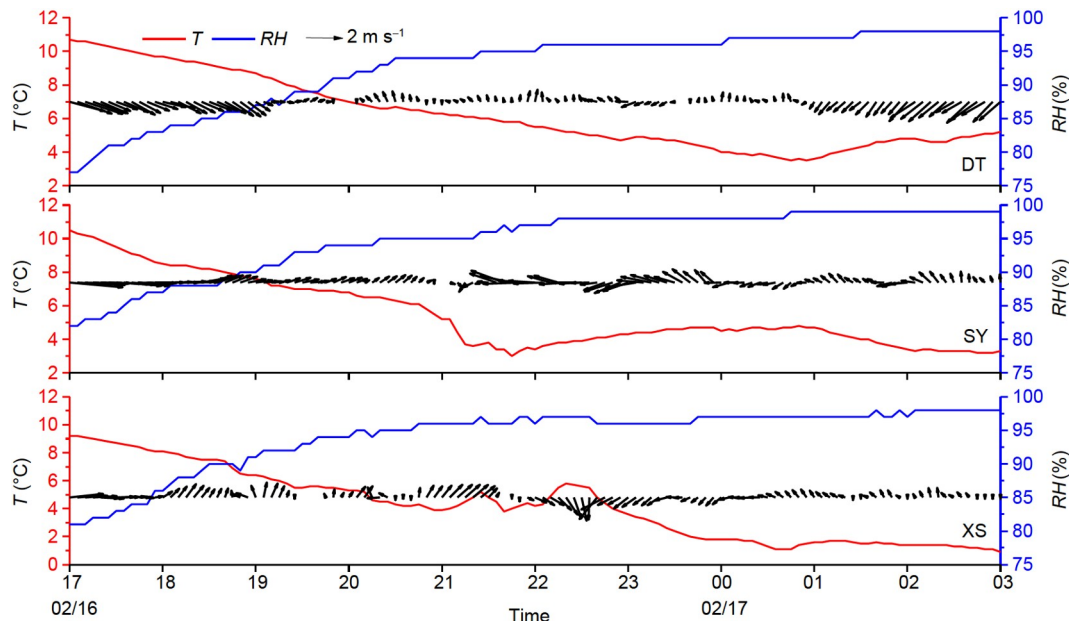
visibility less than 50 m is classified as extremely severe dense fog. Based on above definitions, it is determined that this fog episode in the study area is mainly severe dense fog. In the later stage of the fog episode, extremely severe dense fog appears.

#### 2.4 Observation and identification of sea-land breeze

The sea-land breeze is a typical wind circulation driven by the thermal difference between land and sea (Stull, 1988), which is well known in coastal areas. In order to study the influence of sea-land breeze on fog formation, this study selects three typical coastal stations of Dongtai, Sheyang and Xiangshui in the study area. According to the evolutions of temperature, relative humidity and horizontal wind at different stations over time (Figure 3), the approximate influence periods of land breeze and sea breeze during this fog process are determined. Relevant studies have shown that the formation of sea breeze is usually accompanied by a sudden change in wind direction, an increase in wind speed, a decrease in temperature and an increase in relative humidity (Papanastasiou et al., 2010). As shown in Figure 3, on the evening of February 16, the 10 m easterly wind successively appeared and maintained over Dongtai, Sheyang and Xiangshui, while the surface temperature at each station further decreased. This feature is more prominent in the temperature evolution figures at Sheyang and Xiangshui stations, and the relative humidity at each station also stea-

**Table 1** Physical Parameterization Scheme Settings

Physical process	Parameterization scheme
Boundary layer	YSU (Hong et al., 2006)
Microphysical	Lin (Lin et al., 1983)
Long-wave radiation	RRTM (Mlawer et al., 1997)
Short-wave radiation	New Goddard (Matsui et al., 2020)
Land surface process	Noah (Chen et al., 2010)
Cumulus convective parameterization	Grell 3D (Grell and Dévényi, 2002)

**Figure 3** The evolution of temperature ( $T$ ), relative humidity ( $RH$ ), wind direction, and wind speed (unit:  $m s^{-1}$ ) at 3 meteorological stations of Dongtai (DT), Sheyang (SY), and Xiangshui (XS) in the study area.

dily increases to above 95%, which conforms to the environmental characteristics of the sea breeze formation.

### 3. Results and analysis

#### 3.1 Overview of the severe dense fog process

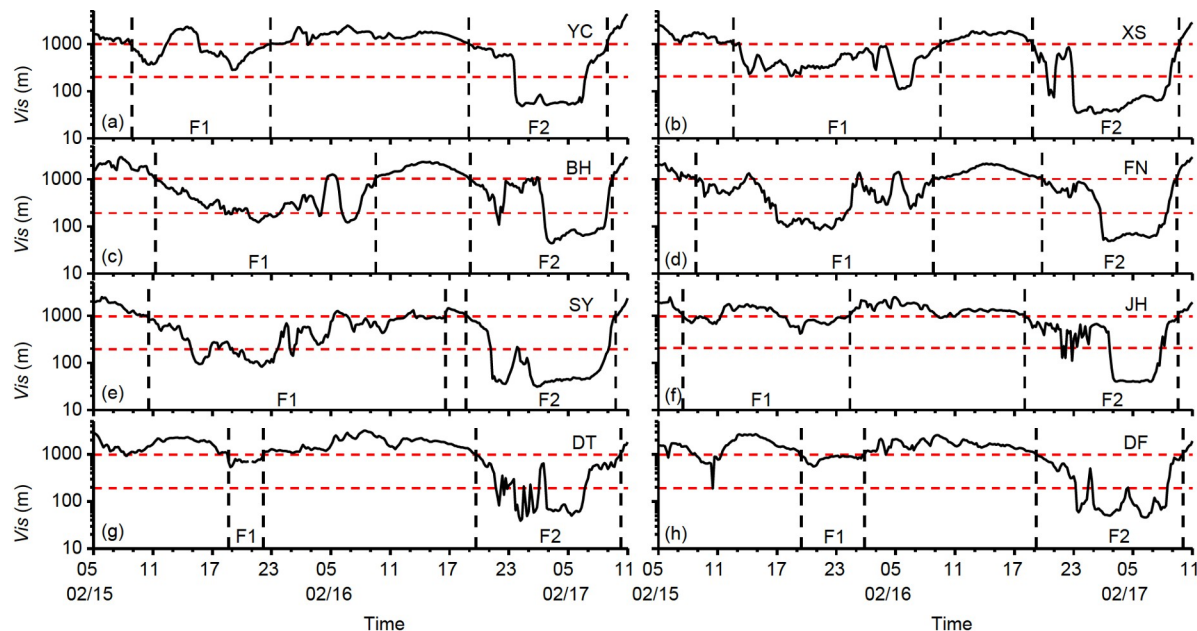
From February 15 to 17, 2015, a persistent severe dense fog process occurred in the study area. The first process began on the morning of February 15, and the fog successively occurred in Jianhu, Funing, Yancheng and Sheyang in the central region of the study area. Subsequently, the fog area developed towards the northern region, affecting Binhan and Xiangshui around noon. After sunset, fog also occurred successively in Dongtai and Dafeng in the southern region. The fog at most stations gradually dissipated until February 16. During this fog process (hereinafter referred to as F1), severe dense fog appeared in Funing, Sheyang, Binhan and Xiangshui, but with short duration. The second process lasted from the night on February 16 to the day on February 17,

which has a long duration, covering the entire Yancheng City. Moreover, the extremely severe dense fog with burst reinforcement characteristics appeared in this stage (hereinafter referred to as F2). More details are listed in Table 2.

Figure 4 shows the visibility evolution at the meteorological stations. On the early morning of February 15, precipitation processes occurred successively at 8 stations in the study area, with sufficient water vapor in the near surface. In the morning, the fog with visibility below 1000 m appeared successively and maintained in Jianhu, Funing, Yancheng and Sheyang. The fog area was mainly located in the central region of the study area. With the fog beginning to form at Binhai and Xiangshui, the visibility at Jianhu and Yancheng increased (Figure 4a and 4f). At this time, the fog region was mainly concentrated at Xiangshui, Binhai, Funing and Sheyang in the central-northern region. After 20:40 BJT, the fog covered the whole study region, with the visibility at Sheyang, Binhai and Funing decreasing below 200 m. After 05:30 BJT on February 16, the fog at Xiangshui became severe dense fog. After 08:40 BJT, the visibility at

**Table 2** The beginning to ending time and duration of F1, F2 and the burst reinforcement stages of F2 at 8 meteorological stations in the study area in 2015

Station	The beginning to ending time of F1	Duration of F1	The beginning to ending time of F2	Duration of F2	The burst reinforcement stage of F2	Duration of the burst reinforcement stage of F2
XS	02/15 12:30–02/16 09:40	21 h 10 min	02/16 18:50–02/17 09:50	15 h	02/16 20:10–02/16 21:10,02/16 22:50–02/17 08:50	1 h 10 h
BH	02/15 11:30–02/16 09:30	22 h	02/16 19:10–02/17 09:30	14 h 20 min	02/17 02:30–02/17 09:00	6 h 30 min
FN	02/15 08:50–02/16 08:40	21 h 50 min	02/16 20:00–02/17 09:30	13 h 30 min	02/17 01:40–02/17 08:30	6 h 50 min
SY	02/15 09:50–02/16 16:40	30 h 50 min	02/16 18:50–02/17 09:50	15 h	02/16 21:00–02/17 09:10	12 h 10 min
JH	02/15 07:30–02/16 00:20	16 h 50 min	02/16 18:10–02/17 09:40	15 h 30 min	02/17 02:30–02/17 07:50	5 h 20 min
YC	02/15 08:50–02/15 23:00	14 h 10 min	02/16 19:00–02/17 09:00	14 h	02/16 23:30–02/17 06:50	7 h 20 min
DT	02/15 18:40–02/15 22:10	3 h 30 min	02/16 19:40–02/17 10:20	14 h 40 min	02/16 21:30–02/17 06:50	9 h 20 min
DF	02/15 19:20–02/16 02:00	6 h 40 min	02/16 19:20–02/17 10:10	14 h 50 min	02/16 23:10–02/17 08:30	9 h 20 min

**Figure 4** Visibility evolution of 8 meteorological stations in the study area from 05:00 BJT to 11:00 BJT on February 15, 2015.

Sheyang, Binhai and Xiangshui increased successively. At 16:40 BJT, the visibility at Sheyang exceeded 1000 m, and the F1 process ended (Figure 4e).

From 18:10 BJT to 19:40 BJT on February 16, the visibility at 8 stations in the study area decreased again to below 1000 m. Xiangshui station experienced its first fog burst reinforcement after the fog forming for over an hour, with the visibility decrease from 551 m to 82 m. The fog developed

into severe dense fog and only lasted for one hour. The large-scale burst reinforcement of fog mainly occurred after 21:00 BJT, and multiple burst reinforcement processes occurred at several stations in the study area. After 02:50 BJT on February 17, the fog became severe dense fog with the visibility below 200 m at all stations. From Figure 4, it can be seen that the visibility curves at different stations all present sharp drop. Yan et al. (2018) pointed out that the burst reinforce-

ment of fog at most stations shows rapid formation of severe dense fog without undergoing the stages of fog and dense fog. In the F2 process of this study, the fog has rapidly developed from dense fog to severe dense fog. After 10 to 50 minutes, the fog at some stations has further developed into extremely severe dense fog with the visibility below 50 m. It maintained from 40 minutes to 6 hours, and the lowest visibility of 31 m appeared at Sheyang station. After 09:00 BJT on February 17, the fog gradually dissipated from south to north, and the visibility at all stations increased to over 1000 m at 10:20 BJT. Then, the severe dense fog process lasting for nearly three days ended.

From the above, we find the difference of fog formation time between the stations during the F1 fog process is relatively long, and the duration of the severe dense fog stage is not long. During the F2 fog process, the difference of fog formation time between the stations is relatively short, and each station experienced fog burst reinforcement.

### 3.2 Synoptic background

At 20:00 BJT on February 14, 2015, a cold vortex moved eastward and southward in high latitudes at 500 hPa. In the middle and low latitudes to the south of Lake Baikal, a trough deepened and moved eastward. At this time, the trough is located in the Hetao area, and the study area is affected by the southwesterly airflow behind the ridge and in front of the trough. At 08:00 BJT on February 15, the temperature trough overlapped with the geopotential height trough at 500 hPa, and the southwesterly airflow in front of the trough moved eastward and northward, accompanied by the large humidity region (Figure 5a1). The southerly meridional wind dominated at upper levels (Figure 5b1). The westerly-southwesterly wind at the bottom of cyclonic circulation dominated at 700 and 850 hPa (Figure omission), which continuously transported warm-moist airflow to the study area, forming a deep moist layer. For the sea level pressure, at 20:00 BJT on February 14, there was a strong cold high pressure in the Altai Mountains. The leading edge of the cold front was located in the area of Inner Mongolia-Ningxia-northwestern Shanxi. At the bottom and in front of the cold high pressure, there was a low pressure center located in Guiyang-Chengdu. The study area was always in the front of the surface low pressure, and was affected by the southerly-southwesterly wind. Under the above circulation situation, weak precipitation began to appear in the whole city from the early morning of February 15.

As the low-pressure inverted trough extended towards northeastward, the study area was located near the southeast side of the inverted trough at 08:00 BJT on February 15 (Figure 5c1). By 20:00 BJT on February 15, the airflow over 500 hPa flattened, and the original southerly wind was gradually replaced by the weak northerly wind from northwest

to southeast (Figure 5b2), with an average wind speed of less than  $2.5 \text{ m s}^{-1}$ . The leading edge of the cold front arrived at the region of Shandong-Henan-Anhui. The study area was located at the back of the low pressure over the sea, and was affected by the northwesterly wind. At this time, the precipitation in most areas gradually stopped. At 08:00 BJT on February 16, the northern branch trough deepened, and a closed cold vortex formed in the central Inner Mongolia. Short wave trough activity was still dominant at 500 hPa, and at the corresponding 700 and 850 hPa the airflow gradually turned into northwesterly airflow behind the trough. The temperature trough lagged behind the height trough, with obvious cold advection. The surface cold high split into two parts of middle-path cold high and west-path cold high. Affected by the cyclone over the sea, the wind in the study area has significantly enhanced, destroying the atmospheric stable stratification and improving the visibility.

By 20:00 BJT on February 16 (Figure 5a2), the 500 hPa was controlled by the northwesterly airflow behind the trough, and the cold advection corresponding to the northwesterly wind at the middle and low levels weakened. The middle-path cold high had moved eastward and southward to the Lake Baikal area and strengthened, and the cold front was located over the region of central Inner Mongolia-Beijing-Liaoning. Under the improvement of sky conditions, the surface radiation cooling at night increased, accompanied by the infiltration of weak cold air. At this time, fog developed throughout the city. As the surface wind gradually turned to easterly wind (Figure 5c2), there was water vapor transport from the sea surface and cold advection cooling, resulting in a large-scale burst reinforcement of fog. After 08:00 BJT on February 17, as the cold high strengthened and moved eastward, the surface wind speed and the surface temperature increased, and the fog began to dissipate.

According to the above analysis, the F1 process is rain fog, and the F2 process is radiation-advection fog.

### 3.3 Evolution characteristics of meteorological elements in the severe dense fog process

According to past studies, the fog occurrence is usually accompanied by stable inversion stratification, and cooling and humidification are also important factors for fog formation and development. However, the cooling in F1 before and after the formation of rain fog was not significant. Before the fog formation, the surface temperature at most stations displayed a slight increase, while at some stations it still showed an increasing trend after the fog formation. Figure 6 shows the temporal evolutions of surface temperature, visibility and precipitation observed at the basic meteorological stations during the F1 process. The warming before the formation of rain fog occurred on the morning of February 15, 2015. At 08:00 BJT on February 15, the sounding at Sheyang station

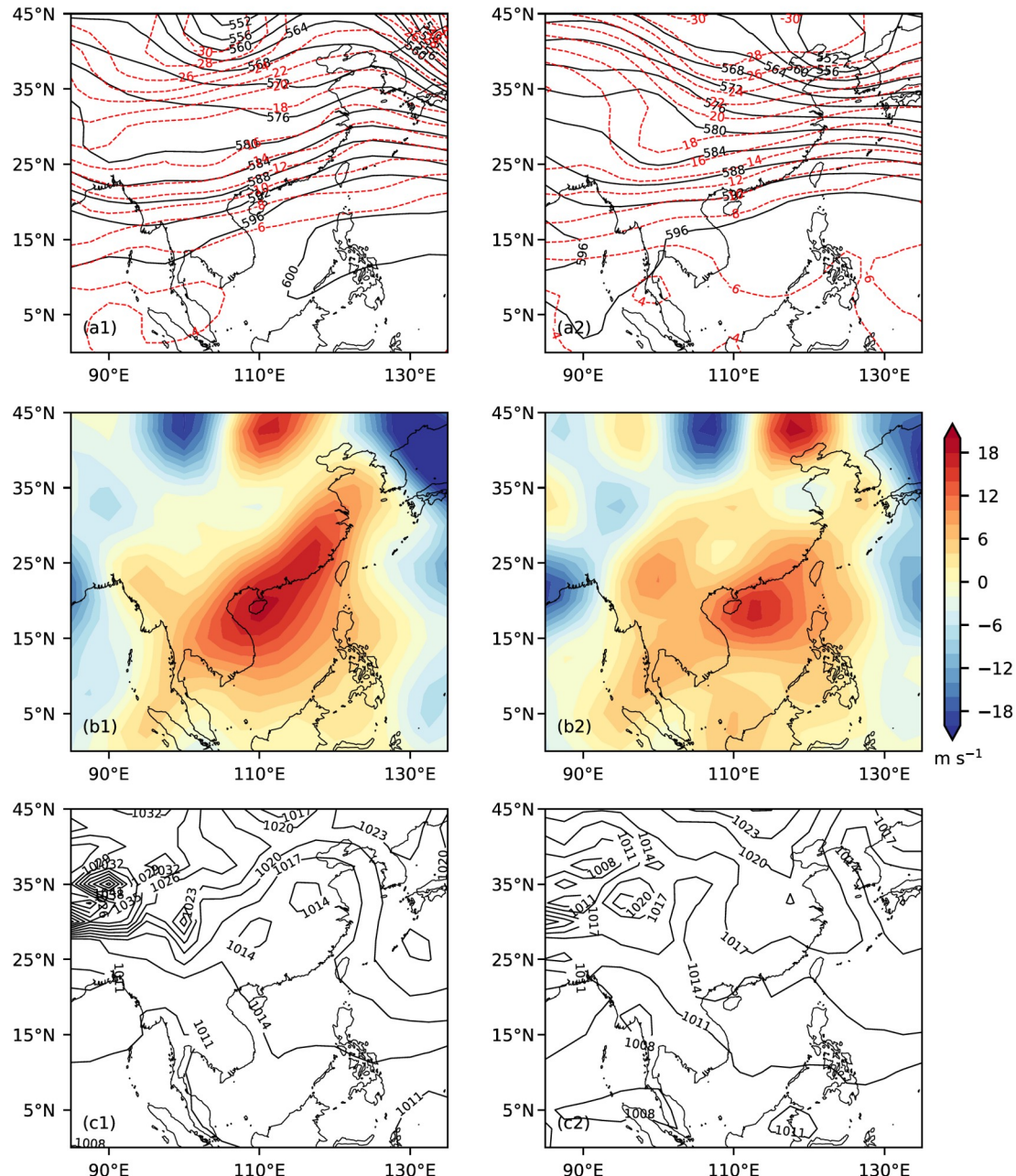


**Figure 5** (a1), (a2) 500 hPa altitude field (black solid line, unit: dagpm) and temperature field (red dashed line, unit: K) and (c1), (c2) sea level pressure field (black solid line, unit: hPa) at 08:00 15th and 20:00 16th on February, 2015. (b1), (b2) the average meridional wind speed at 500 hPa (shadow: positive values for southerly winds and negative values for northerly winds; contour line: equal wind speed line, unit:  $m s^{-1}$ ) at 08:00 and 20:00 on February 15, 2015.

(Figure omitted) displayed that there was a shallow inversion layer near the surface. At the same time, a weak precipitation process appeared in the study area on February 15, and the coverage of precipitation clouds led to a decrease in surface radiation and an increase in atmospheric counter radiation. These features help maintain the temperature near the surface, leading to a slight increase in surface temperature during the early stages of rain fog formation. The temperature increase after the fog formation was mainly due to the enhanced condensation nucleation effect with the precipita-

tion enhancement. According to observation data, the precipitation first appeared in Jianhu from 02:00 BJT on February 15, and the precipitation area covered the entire city at 07:00 BJT. The heaviest rainfall was concentrated between 08:00 BJT and 12:00 BJT, and the rainfall gradually stopped in most areas after 12:00 BJT. As the rainfall increased after 08:00 BJT, raindrops continued to fall and evaporate, maintaining a saturated state near the surface. The water vapor in the fog continued to condense and nucleate, releasing latent heat to cause a slight increase of surface

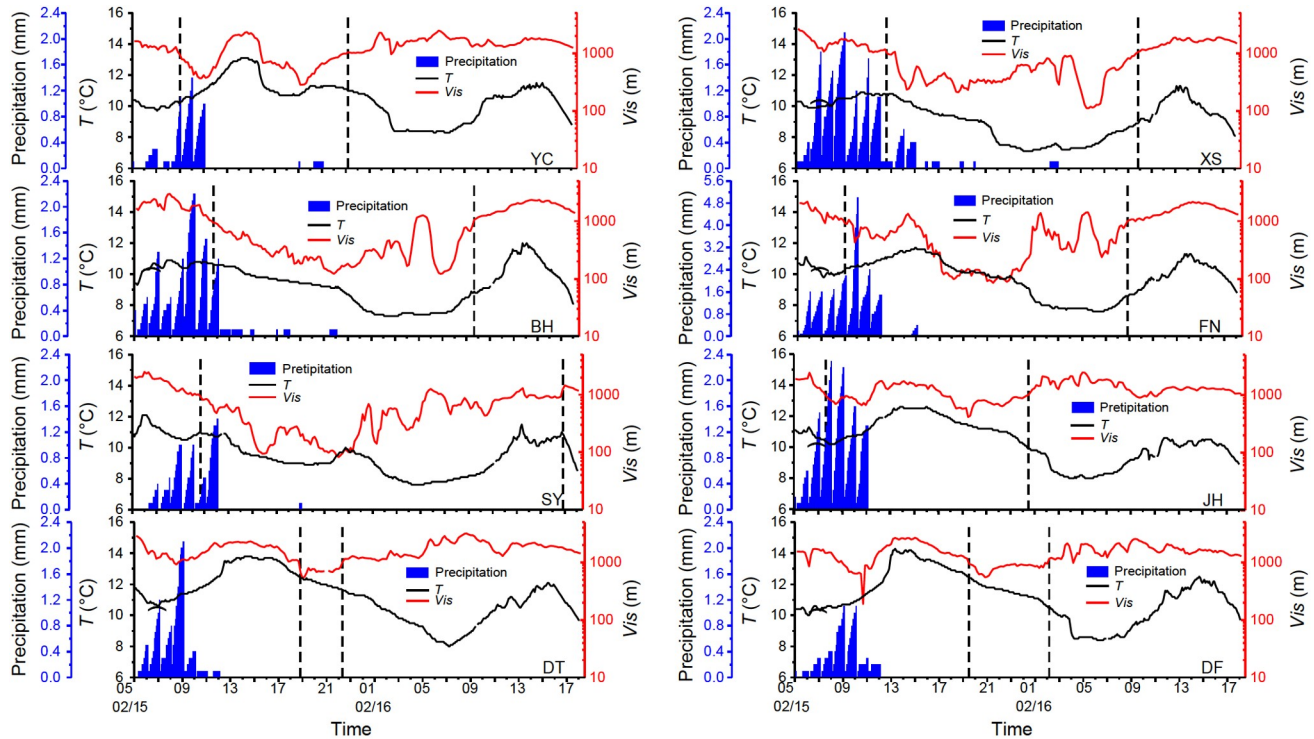


**Figure 6** The evolution of surface temperature, visibility, and precipitation at 8 meteorological stations in the study area from 05:00 to 18:00 on February 15, 2015.

temperature. Exactly as Yan et al. (2010) proposed, the essence of rain fog is evaporation fog. The difference is that the short-term enhancement of rainfall intensity during the studied rain fog process can easily lead to a short-term improvement in visibility. However, although the enhancement of rainfall intensity during the F1 process can result in small fluctuations of visibility, it still presented a decrease trend overall.

At Yancheng station, from the vertical profile of temperature advection (Figure 7a) and the 10 m wind field (Figure 7b) during the rain fog period, it can be seen that during the initial time of rain fog the surface wind speed was less than  $1.5 \text{ m s}^{-1}$ , the wind direction was mainly easterly-southeasterly, and the near-surface warm advection was significant (more than  $6 \times 10^{-5} \text{ K s}^{-1}$ ). After 11:00 BJT, the surface wind gradually turned to northwesterly wind, and the low-level warm advection weakened. The wind speed increased to around  $3 \text{ m s}^{-1}$ . The increase in wind speed made the original weak stable stratification unstable, and the rain fog dissipated temporarily. After 15:00 BJT, the surface wind turned to weak northeasterly wind, and the easterly wind component was conducive to the transport of water vapor from the sea. Weak cold air at upper levels further infiltrated into low levels, and the near surface still maintained a relatively warm and humid environment. The visibility once again decreased to below 1 km. After 19:00 BJT, the surface wind turned into westerly-northwesterly wind. The cold advection infiltrated to the near surface, the wind speed ra-

pidly increased, the northerly component gradually increased, and the rain fog completely dissipated. Meanwhile, the wind field conversion at other stations has the same impact on the temperature advection and visibility variation at the station. Wang et al. (2020) pointed out that during the formation and development stages of rain fog, the low level of the atmospheric boundary layer mainly prevailed weak cold advection, but sometimes there was warm advection. During the F1 rain fog process, there was relatively obvious warm advection in the atmospheric boundary layer at Yancheng station. Until the later stage on February 15, the rain fog began to dissipate after the warm advection gradually turned to cold advection.

For the F2 radiation-advection fog process, with the end of the precipitation process on February 15, the weather in the whole city turned fine on February 16. The distribution of meteorological elements at different time in the study area is shown in Figure 8. The surface temperature continued to increase from morning to around 10:00 BJT, and the early precipitation still provided good humidity conditions for the underlying surface in the study area, with a relative humidity above 90%. The surface was mainly dominated by westerly wind (Figure 8a). With the enhancement of solar radiation, the evaporation of water vapor near the surface was remarkable, and the relative humidity in most areas decreased, with the lowest relative humidity dropping to 77%. Except for a few coastal stations with small temperature variations, the surface temperature at most other stations significantly

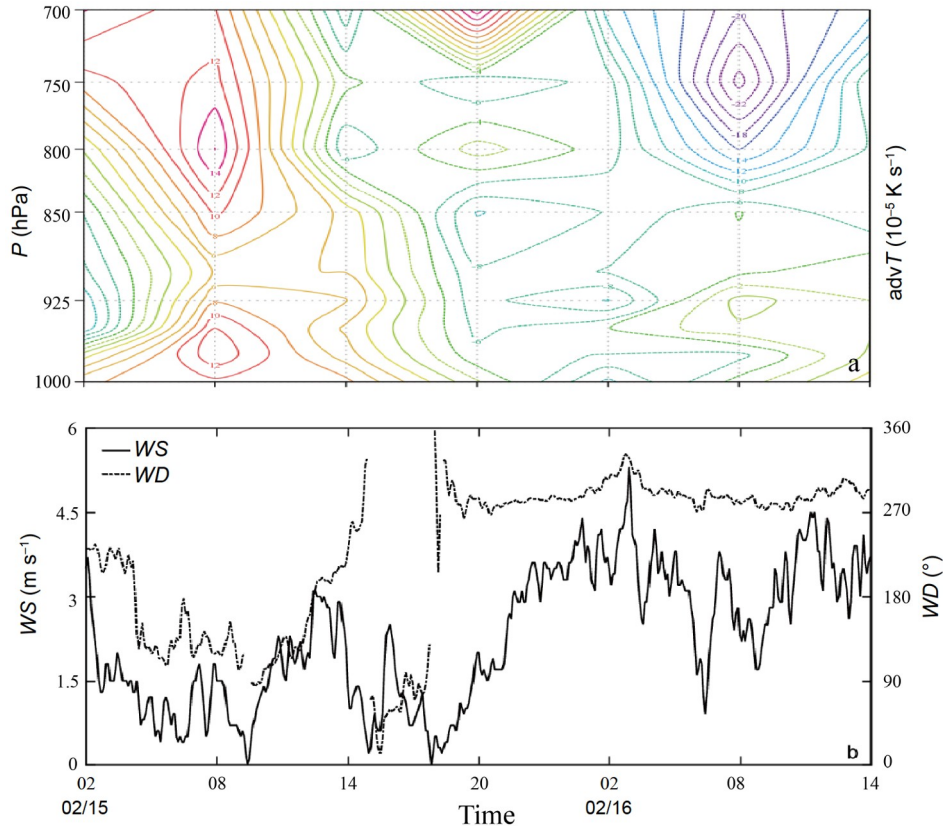


**Figure 7** From 02:00 on February 15, 2015 to 14:00 on February 16, 2015 at Yancheng Station, (a) time-height vertical profile of temperature advection (based on NCEP reanalysis data, unit:  $10^{-5} \text{ K s}^{-1}$ ) and (b) the variation of surface 10 m wind direction ( $^{\circ}$ ) and wind speed ( $\text{m s}^{-1}$ ) over time.

increased, with the maximum temperature of around  $12^{\circ}\text{C}$ . Therefore, the study area maintained a relatively warm underlying surface (Figure 8b). After 15:00 BJT, as the cyclone over the sea moved away, the near-surface wind speed gradually decreased, even being calm wind at some time (Figure 8c). The wind direction at some coastal stations gradually turned to northeasterly wind. With the establishment of sea breeze, the near-surface humidity conditions were improved, which was conducive to the formation of radiation-advection fog (Liu et al., 2014). After 19:00 BJT, the fog gradually developed throughout the city, and the surface wind at each station gradually shifted to easterly wind, which was conducive to the transportation of water vapor from the sea surface to the study area. The relative humidity in most areas exceeded 90% in succession, and the surface temperature dropped to  $5\text{--}7^{\circ}\text{C}$  (Figure 8d). After 21:00 BJT, each station entered the fog burst reinforcement stage, and the surface wind remained mainly easterly wind. The relative humidity in the study area was increased to over 95%, and the surface temperature further decreased (Figure 8e). By around 03:00 BJT on February 17, the whole city was in the stage of severe dense fog, and the relative humidity at each station kept the high values above 97%. The wind field gradually shifted from easterly to southerly (Figure 8f). According to the above analysis, it can be seen that during this persistent se-

vere dense fog process, the cooling was not significant in the early rain fog process, but was a favorable condition for the formation of radiation-advection fog in the later stage (Pu et al., 2008b).

#### 4. Cause analysis of fog burst reinforcement

In this section, we use the mesoscale WRF model to simulate the F2 fog process. The simulation results and the retrieval of fog area from the MTSAT (multi-functional transport satellite) data are compared with the observations (Figure 9). The bright temperature difference of  $3.9 \mu\text{m}$  and  $12.4 \mu\text{m}$  channels less than 2 K is defined as fog. The dual channel interpolation method is suitable for the nighttime fog retrieval (Wang et al., 2018). The observation shows that, the development of fog in coastal areas was rapid, and the fog area continued to extend inland, developing into a large-scale severe dense fog. The fog area retrieved by the MTSAT data also shows the characteristics of fast spreading from southeast to northwest. The distribution of fog area simulated by the WRF shows that the fog evolution trend is basically consistent with the observations. At 20:00 BJT on February 16, fog had already formed in the eastern coastal area, and then the fog spread from east to west. The propagation di-

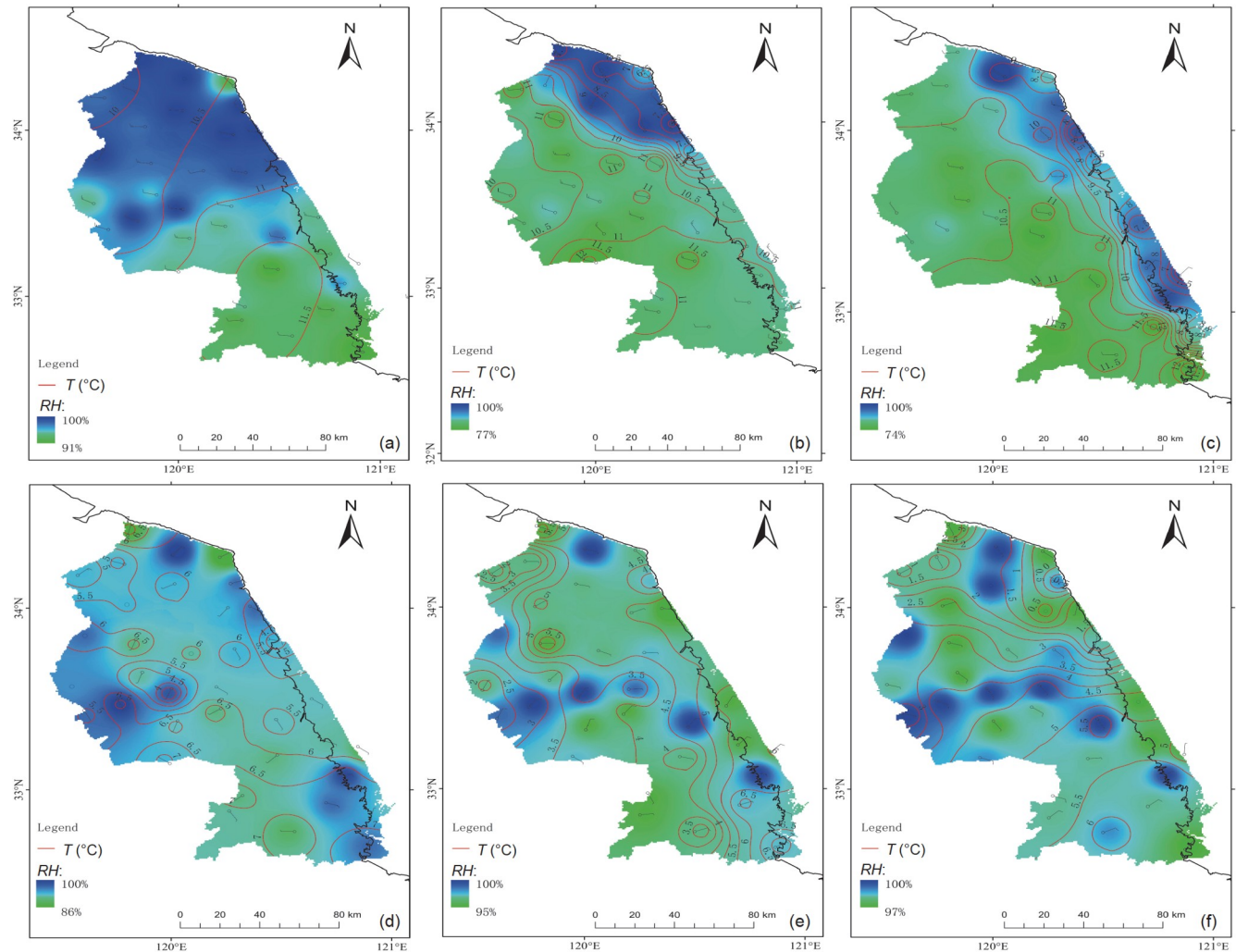


**Figure 8** In February 2015 (a) at 09:00 on the 16th; (b) at 13:00 on the 16th; (c) at 16:00 on the 16th; (d) at 20:00 on the 16th; (e) at 00:00 on the 17th; (f) at 03:00 on the 17th, the distribution of wind field ( $\text{m s}^{-1}$ ), temperature ( $^{\circ}\text{C}$ ) and relative humidity (%) at basic stations and regional stations in the study area (the black solid line in each picture is the coastline, and the color area on the right side of the coastline is the mudflat).

rection was basically parallel to the coastline, that is, it developed from coastal to inland. After 10:00 BJT on February 17, the observation displays that the fog area dissipated extensively, and the corresponding simulated fog area also significantly decreases. In general, the WRF model has accurately simulated the fog evolution process, and the simulation results are credible to a certain extent.

On this basis, in order to further evaluate the simulation effect of WRF model on the process of fog burst reinforcement, we calculate and output the hourly visibility (Figure 10) at each station during the F2 fog process based on the following equation (Kunkel 1984):  $Vis=27\times LWC^{0.88}$ . Compared with the observational visibility (Figure 4), when there is no fog (the visibility is greater than 1000 m), the simulated visibility is close to infinity; when there is fog or dense fog (the visibility is greater than 200 m but less than or equal to 1000 m), the simulated visibility differs greatly from the observation; however, when the observation enters the stage

of fog burst reinforcement (the visibility rapidly drops to below 200 m), the corresponding simulated visibility also drops sharply to below 200 m, exhibiting obvious burst reinforcement characteristics. As can be seen, for the F2 fog process, the WRF model can effectively simulate the visibility variation characteristics of fog burst reinforcement. Therefore, conducting physical analysis of fog burst reinforcement based on the simulation output is also reasonable.

Seen from the 10 m wind simulation, the coastal areas gradually turn to easterly wind from 18:00 BJT on February 16. At 22:00 BJT, the whole city is affected by sea breeze, and the fog burst reinforcement occurs at each station successively. Compared with Figure 9, it can be seen that the simulated fog area covers the research area at this time. By 02:00 BJT on February 17, most areas of Jiangsu Province turn to easterly-northeasterly wind. Under the continuous influence of sea breeze, the simulated fog area covers the

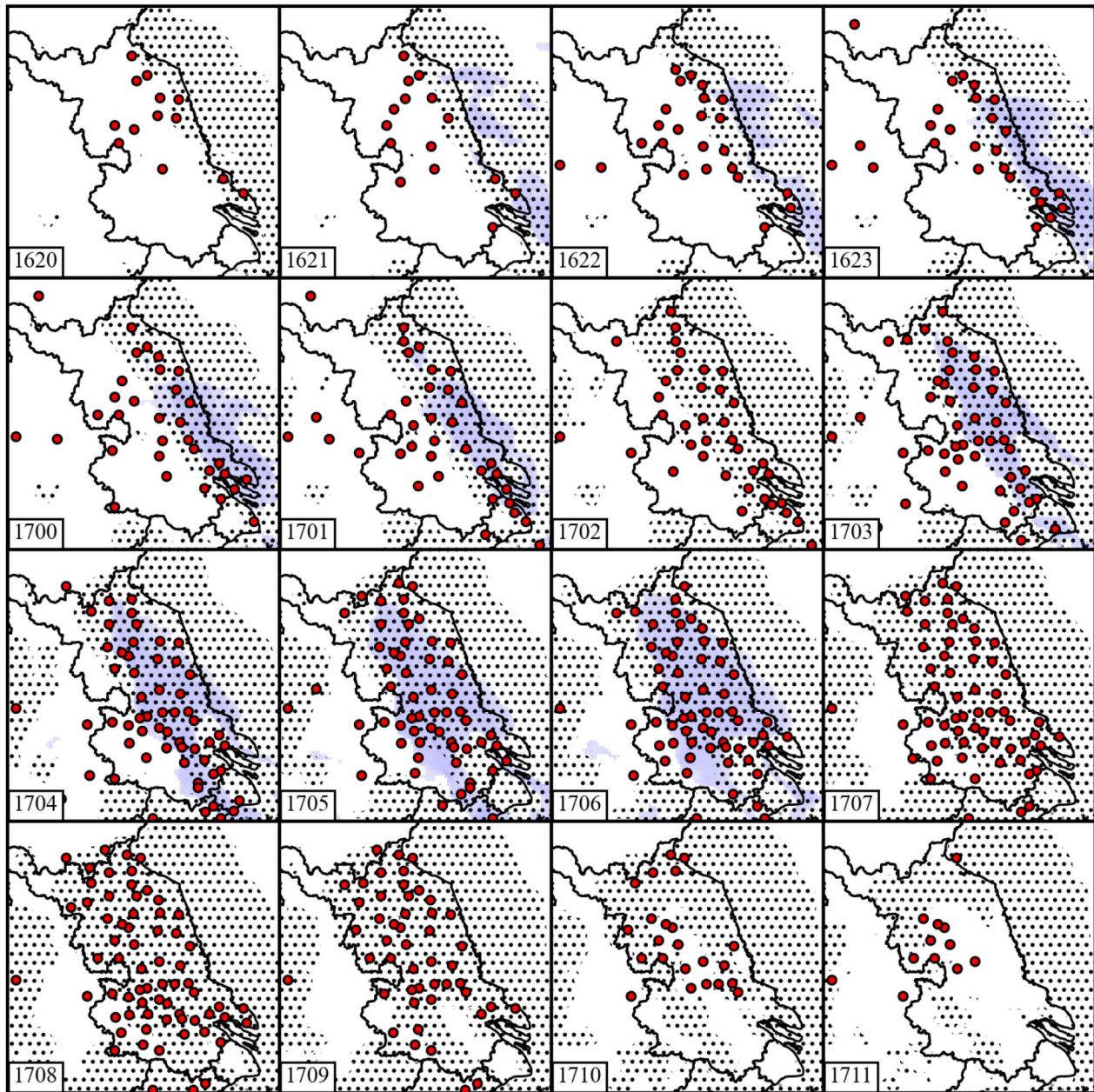


**Figure 9** The distribution of fog area simulated by the WRF (black dots), the retrieval of fog area from the MTSAT data (blue shadow from 20:00 on February 16 to 06:00 on February 17, 2015, lacking satellite data at 02:00 on February 17), and the observation of fog area (red dots). 1620 is 20:20 on February 16, the same below.

central-eastern Jiangsu Province. The simulated visibility (Figure 10) shows that there is severe dense fog in the study area. In order to verify that the conversion of sea breeze and land breeze has a certain impact on the fog development, this section uses the WRF simulation experiments to carry out specific analysis. In this simulation experiment, the following two line segments are selected to make meridional-vertical cross-sections (Figure 11b). The first line segment is between Xilian Island and Dongzaogang stations (red line), and it is deemed as the “coastal line” which passes through the coastal areas of Xiangshui, Binhai, Sheyang, Dafeng and

Dongtai. The second line segment connects Dafeng, Yangcheng and Jianhu stations (blue line), and it is deemed as the “coast-to-inland line”.

The cross-section along the “coastal line” (Figure 12) shows that, there is consistent westerly-northwesterly wind from 0 m to 800 m at 14:00 BJT on February 16. The solar radiation causes a small increase of temperature in most areas along the coastal line and an increase of temperature difference between sea and land, which is conducive to the establishment of sea breeze. At 17:00 BJT, the surface at Sheyang, Dafeng and Dongtai along the coastal area of the

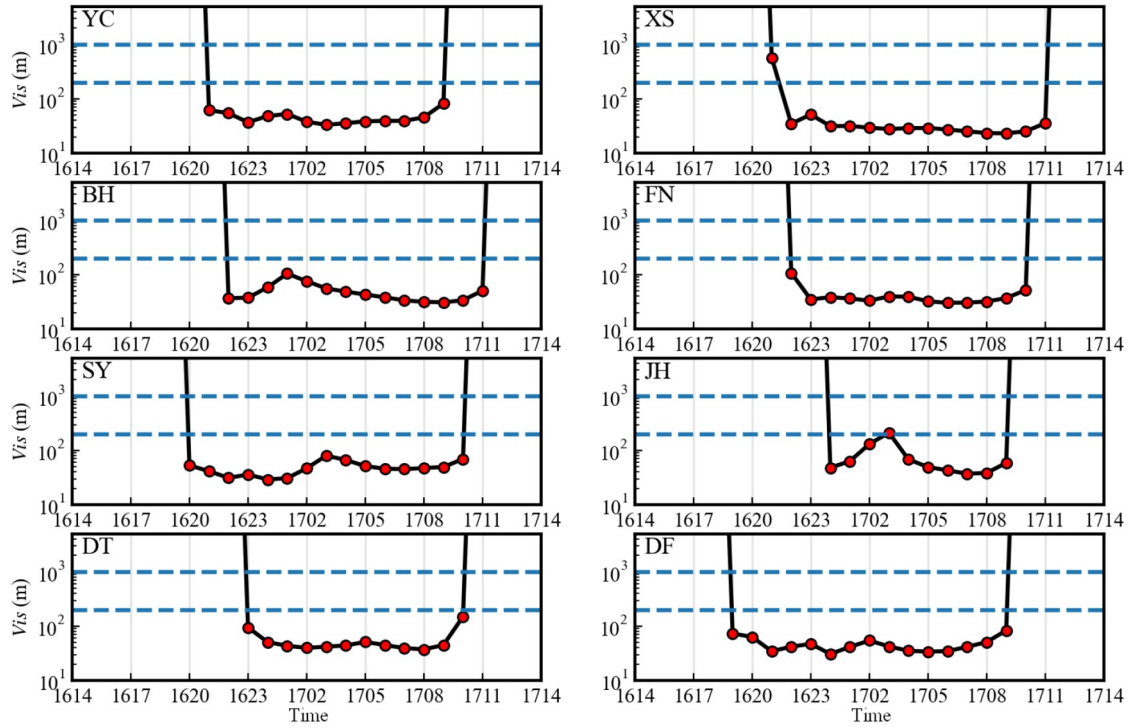


**Figure 10** Visibility evolution of 8 meteorological stations in the study area simulated by WRF from 14:00 16th to 14:00 17th on February, 2015.

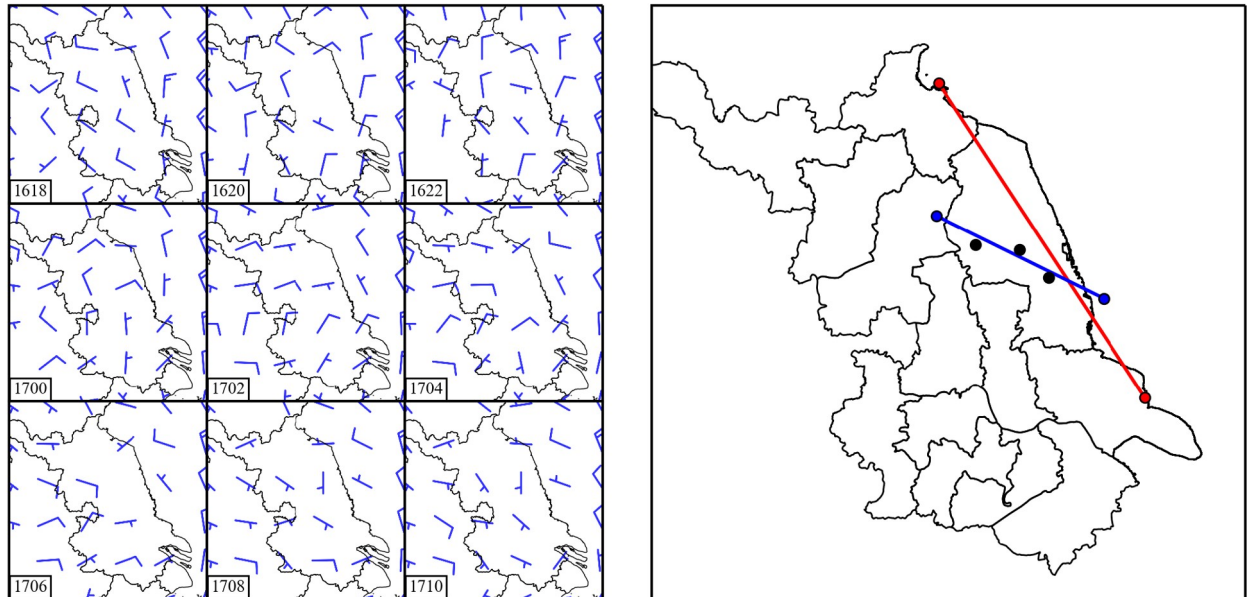


**Figure 11** (a) 10 m wind field (unit:  $\text{m s}^{-1}$ ) simulated by WRF from 18:00 16th to 10:00 17th on February, 2015 and (b) the stations of meridional-vertical cross-sections (red solid line: coastal line; blue solid line: coast-to-inland line).

study area first turns to northeasterly wind. The area above 50 m is still dominated by northerly-northwesterly wind. Affected by the weak cold advection of the sea breeze, the surface temperature at Sheyang, Dafeng and Dongtai substantially decreases. As a result, there is an overhang inversion, with an inversion intensity of about  $1.5 \text{ }^\circ\text{C (100 m)}^{-1}$ .

At 18:00 BJT, the surface layer at Xiangshui and Binhai also turns to sea breeze, and the surface inversion gradually forms, with an inversion intensity of about  $1 \text{ }^\circ\text{C (100 m)}^{-1}$ . The overhang inversion above Sheyang, Dafeng and Dongtai also further develops into surface inversion. The fog in the coastal area of the study area gradually develops. According

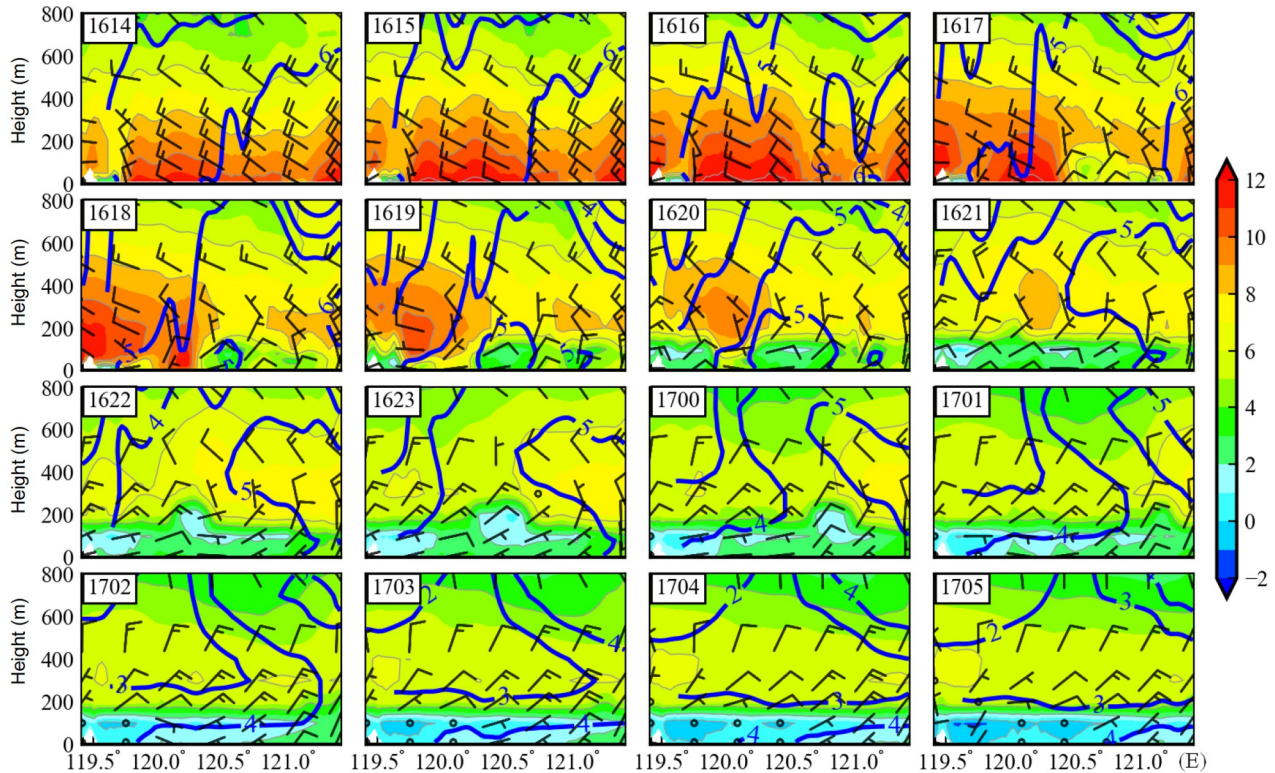


**Figure 12** The meridional-vertical cross-sections along the red solid line in Figure 11b simulated by WRF from 14:00 16th to 05:00 17th on February, 2015. Blue contour line: saturated specific humidity (unit:  $\text{g kg}^{-1}$ ); Stain: temperature (unit:  $^{\circ}\text{C}$ ); Wind rod (unit:  $\text{m s}^{-1}$ ).

to the cross-section along the “coast-to-inland line” (Figure 13), by 19:00 BJT, the fog layer at Dafeng has developed to the height of about 200 m, while the near-surface layer at Yancheng and Jianhu (located in the inland area) is still dominated by northerly-northwesterly wind. After 20:00 BJT, the area below 200 m in the coastal area turns from land breeze to sea breeze, with the wind speed decreased. The continuous transport of weak cold advection at low levels help maintain a stable stratification (warm at upper level and cold at low level) in the study area, which is conducive to the maintenance of the inversion layer. The thickness of the inversion layer exceeds 400 m and the intensity is strengthened (reaching  $2^{\circ}\text{C (100 m)}^{-1}$ , which is favorable for the fog burst reinforcement in the coastal area (Zhang et al., 2014).

As the sea breeze develops from east to west, the fog area obviously expands from coast to inland. After 00:00 BJT on February 17, the level below 600 m in the study area is affected by easterly-northeasterly wind (Figure 13), and the whole city is in the fog area, with the fog layer thickness of 300 m. There is an obvious large wind speed area near the fog top, with the wind speed reaching  $6\text{--}8 \text{ m s}^{-1}$ . Andreas et al. (2000) considered that when the maximum wind speed at low levels exceeds the minimum wind speed above and below this level by more than  $2 \text{ m s}^{-1}$ , it is defined as a low-level jet. Jin et al. (1983) analyzed the characteristics of meteorological elements at the tower layer (320 m), and

pointed out that when the maximum wind speed below the tower layer exceeds  $5 \text{ m s}^{-1}$  and when the wind speed difference between the upper and lower levels exceeds  $1.5 \text{ m s}^{-1}$ , it can be defined as an ultra-low level jet. Shen et al. (2022) emphasized that the ultra-low level jet is conducive to the transport of water vapor in the atmospheric boundary layer. At this time, the wind speed near the fog top is significantly higher than the wind speed at upper and lower layers, and the height of fog top is around 300 m, which satisfies the standard of ultra-low level jet. The occurrence of easterly jet leads to a decrease in the fog top height, but the cooling rate at the near surface layer increases. The inversion intensity below the fog top further strengthens. In addition, the easterly wind transports water vapor from the sea surface to the study area, accelerating the burst reinforcement of fog.

Ding and Liu (2014) pointed out that the variations of relative humidity in eastern China are closely related to the actual specific humidity (water vapor supplied from the sea surface) and saturated specific humidity (near surface temperature). The L-band radar sounding at Sheyang station (Figure 14a) shows that at 20:00 BJT on February 16, there was an inversion layer near the surface, with the intensity close to  $1^{\circ}\text{C (100 m)}^{-1}$ . The thickness of the inversion layer was thin, only about 106 m. At this time, the actual fog top height was lower than the thickness of the surface inversion layer, but the low-level wind field was dominated by wes-

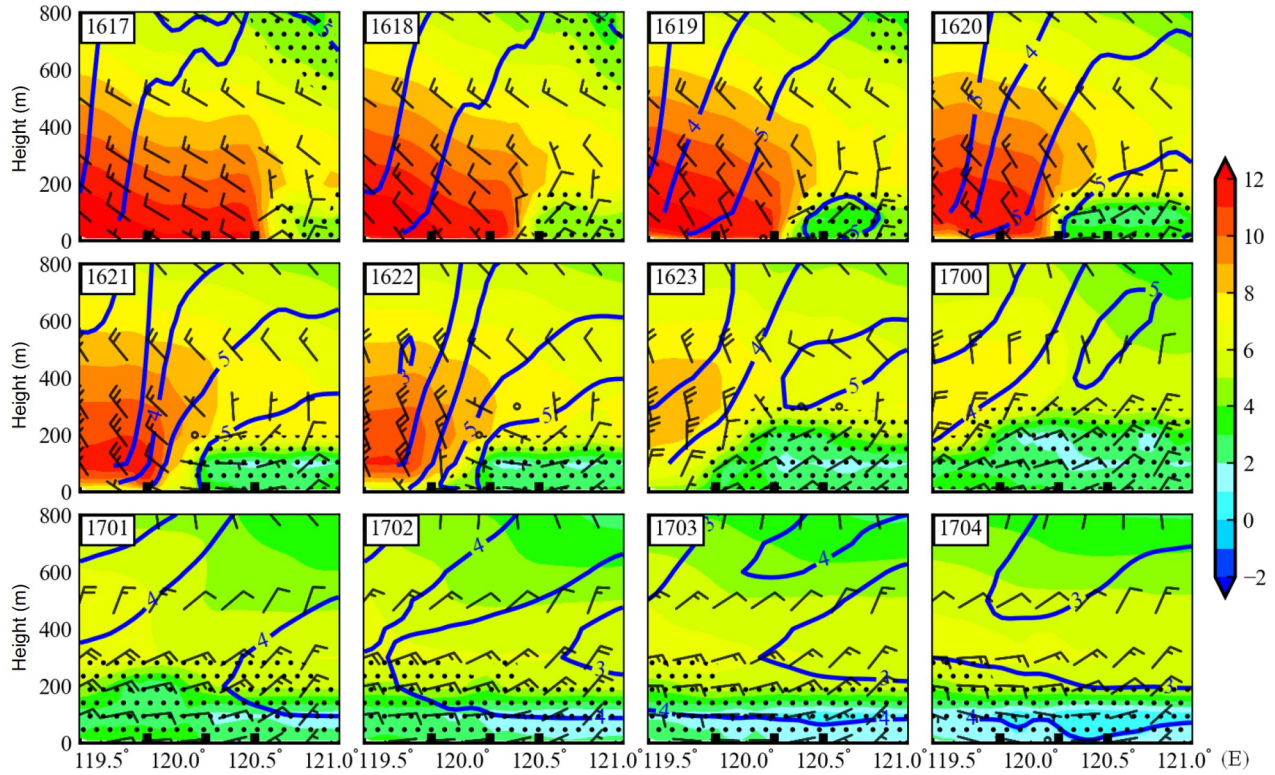


**Figure 13** The meridional-vertical cross-sections along the blue solid line in Figure 11b. Simulated by WRF from 17:00 16th to 04:00 17th on February, 2015. Blue contour line: saturated specific humidity (unit:  $\text{g kg}^{-1}$ ); Stain: temperature (unit:  $^{\circ}\text{C}$ ); Black scatter: fog area; Wind rod (unit:  $\text{m s}^{-1}$ ).

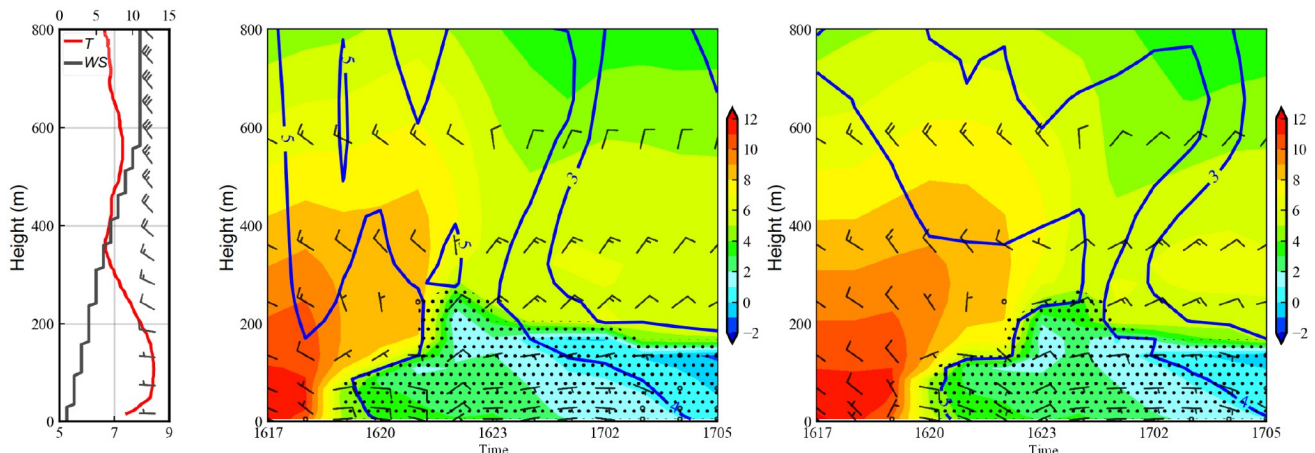


**Figure 14** (a) The temperature ( $T$ ), wind direction, and wind speed ( $WS$ ) vertical profile of the L-band radar sounding at Sheyang station ( $33.46^{\circ}\text{N}, 120.15^{\circ}\text{E}$ ) at 20:00 BJT on February 16, 2015. The time-height cross-section (b) at the Sheyang Station and (c) Yancheng Station. Blue contour line: saturated specific humidity (unit:  $\text{g kg}^{-1}$ ); Stain: temperature (unit:  $^{\circ}\text{C}$ ); Black scatter: fog area; Wind rod (unit:  $\text{m s}^{-1}$ ).

terly wind. According to the time-height cross-section at the Sheyang station (Figure 14b) simulated by the WRF, the surface inversion layer begins to form at night on February 16. At 20:00 BJT, the fog area develops to around 100 m, which is smaller than the thickness of the surface inversion layer and is well consistent with the observation. Figures 14b and 14c present the time-height cross-sections of the simulated wind, temperature and saturated specific humidity at the coastal station (Sheyang) and inland station (Yancheng).

As can be seen, under the cooling effect of sea breeze advection, the temperature at the near-surface layer in the study area gradually decreases, causing the saturated specific humidity at low levels to decrease from  $5 \text{ g kg}^{-1}$  to below  $4 \text{ g kg}^{-1}$ . At the same time, the water vapor from the sea surface is still continuously transported to the study area. This indicates that the actual specific humidity increases. Therefore, the relative humidity also significantly increases over the study area and maintains at high values, providing

sufficient water vapor conditions for the fog to maintain in the burst reinforcement stage for a long time.

[Bushahab et al. \(2009\)](#) pointed out that under the background of clear radiance at night, the water vapor continuously transported by the sea breeze in the afternoon can quickly reach saturation and condense, which is conducive to the fog formation. [Zhu et al. \(2018\)](#) studied the triggering factors for the fog burst reinforcement, and pointed out that the wind direction transition from land-lake breeze to lake-land breeze in autumn and winter will lead to an increase in land surface humidity and a significant decrease in temperature. They also showed that the burst reinforcement in visibility often occurs after 15:00 BJT. In the F2 process, the influence of the sea-land breeze transition on the fog formation is reflected in two aspects. On one hand, the establishment of the near-surface sea breeze is conducive to the advection cooling at low levels, which leads to the occurrence and maintenance of the overhang inversion and the surface inversion, promoting the formation and development of fog. On the other, with the increase of sea breeze circulation, water vapor is continuously transported from the sea surface to the study area, and the occurrence of the ultra-low level jet makes the water vapor accumulate in the near surface layer. Meanwhile, the inversion intensity is further strengthened, which is favorable for the burst reinforcement and long-term maintenance of fog.

## 5. Conclusions

Through the observation and simulation of the influence of sea-land breeze on the severe dense fog in the coastal area of the Yellow Sea, the following conclusions are drawn.

(1) This persistent severe dense fog process occurred under the circulation background of frequent upper-level trough and eastward-moving vortices at middle and low levels. The precipitation caused by the southwesterly airflow in front of the upper-level trough and the low-pressure inverted trough are conducive to the formation of early rain fog, while the nighttime clear radiance under the control of surface cold high and the infiltration of weak cold advection are conducive to the formation and development of later radiation-advection fog.

(2) For this rain fog process, the short-term enhancement of rainfall intensity leads to a fluctuation decrease in visibility. It is different from the characteristic of most previous rain fog processes in which the enhancement of rainfall intensity improves the visibility. As can be seen, the relationship between the rainfall intensity and visibility variation during this rain fog process is not significant. During the period of severe dense fog, the cooling is not obvious during the early rain fog process, providing favorable conditions for the formation of radiation-advection fog. Although the

thickness of the saturated moist layer of radiation-advection fog is significantly lower than that of rain fog, the coordination between the near-surface saturated moist layer and the dry air at middle and upper levels is more conducive to the development and enhancement of this severe dense fog.

(3) The establishment of sea breeze has an advection cooling effect on the near surface layer, leading to the occurrence and maintenance of overhanging inversion and surface inversion, and the stable stratification conditions are conducive to the formation and burst reinforcement of fog. On one hand, the strengthening of sea breeze circulation can continuously transport water vapor to the study area. On the other, the occurrence of ultra-low level jet is favorable for the accumulation of low-level water vapor. At the same time, the inversion intensity further strengthens, which is in favor of the burst reinforcement and long-term maintenance of fog.

In this study, we only analyzed a typical physical process of fog burst reinforcement by using observation data and numerical model. In the future, we need to further understand the impact of sea-land breeze circulation on the burst reinforcement of dense fog in coastal areas. In addition, the complex physical process of atmospheric boundary layer during fog processes needs to be deeply analyzed with high-resolution numerical models and more comprehensive observation of sea-land breeze.

**Acknowledgements** This work was supported by the National Natural Science Foundation of China (Grant Nos. 42075063 & 42075066), the Open Project of State Key Laboratory of Severe Weather (Grant No. 2021LASW-A07), the Jiangsu Meteorological Youth Fund Project (Grant No. KQ202215), the Special Fund for Basic Scientific Research Business of China Academy of Meteorological Sciences (Grant No. 2022Y025), the Bei Ji Ge Open Research Fund (Grant No. BJJ202307), and the Science and Technology Project of Yancheng Meteorological Administration (Grant No. YQK2021016).

**Conflict of interest** The authors declare that there are no conflicts of interest.

## References

- Andreas E L, Claffy K J, Makshtas A P. 2000. Low-level atmospheric jets and inversions over the western Weddell Sea. *Bound-Layer Meteor*, 97: 459–486
- Bendix J, Eugster W, Klemm O. 2011. Fog-boon or bane? *Erdkunde*, 65: 229–232
- Brenguier J L, Pawlowska H, Schüller L, Preusker R, Fischer J, Fouquart Y. 2000. Radiative properties of boundary layer clouds: droplet effective radius versus number concentration. *J Atmos Sci*, 57: 803–821
- Bushahab A, Suwaidi A A, Ghedira H, Mubarak K. 2009. Fog forecasting, detection and monitoring in the UAE using SEVIRI-MSG data. *Geoscience and Remote Sensing Symposium, Geoscience and Remote Sensing Symposium, IEEE International, IGARSS*
- Chen S, Liu D, Kang Z, Shi Y, Liu M. 2021. Anomalous atmospheric circulation associated with the extremely persistent dense fog events over eastern China in the late autumn of 2018. *Atmosphere*, 12: 111
- Chen Y, Yang K, Zhou D, Qin J, Guo X. 2010. Improving the Noah land surface model in arid regions with an appropriate parameterization of

- the thermal roughness length. *J Hydrometeorol*, 11: 995–1006
- Choi H, Speer M S. 2006. The influence of synoptic-mesoscale winds and sea surface temperature distribution on fog formation near the Korean western peninsula. *Meteorol Appl*, 13: 347–360
- Ding Q, Sun J, Huang X, Ding A, Zou J, Yang X, Fu C. 2019. Impacts of black carbon on the formation of advection-radiation fog during a haze pollution episode in eastern China. *Atmos Chem Phys*, 19: 7759–7774
- Ding Y H, Liu Y J. 2014. Analysis of long-term variations of fog and haze in China in recent 50 years and their relations with atmospheric humidity. *Sci China Earth Sci*, 57: 36–46
- Fu G, Guo J, Pendergrass A, Li P. 2008. An analysis and modeling study of a sea fog event over the Yellow and Bohai Seas. *J Ocean Univ China*, 7: 27–34
- Fuzzi S, Facchini M C, Orsi G, Lind J A, Wobrock W, Kessel M, Maser R, Jaeschke W, Enderle K H, Arends B G, Berner A, Solly I, Kruis C, Reischl G, Pahl S, Kaminski U, Winkler P, Ogren J A, Noone K J, Hallberg A, Fierlinger-Oberlinninger H, Puxbaum H, Marzorati A, Hansson H C, Wiedensohler A, Svenssonsson I B, Martinsson B G, Schell D, Georgii H W. 1992. The po valley fog experiment 1989: An overview. *Tellus B-Chem Phys Meteor*, 44: 448–468
- Fuzzi S, Laj P, Ricci L, Orsi G, Heintzenberg J, Wendisch M, Yuszkiewicz B, Mertes S, Orsini D, Schwanz M, Wiedensohler A, Stratmann F, Berg O, Swietlicki E, Frank G, Martinsson B, Günther A, Dierssen J, Schell D, Jaeschke W, Berner A, Dusek U, Galambos Z, Kruis C, Mesfin N, Wobrock W, Arends B, Brink H. 1988. Overview of the Po valley fog experiment 1994 (CHEMDROP). *Contrib Atmosph Phys*, 71: 3–19
- Goodman J. 1977. The microstructure of California coastal fog and stratus. *J Appl Meteor*, 16: 1056–1067
- Grell G A, Dévényi D. 2002. A generalized approach to parameterizing convection combining ensemble and data assimilation techniques. *Geophys Res Lett*, 29: 1693
- Gultepe I, Tardif R, Michaelides S C, Cermak J, Bott A, Bendix J, Müller M D, Pagowski M, Hansen B, Ellrod G, Jacobs W, Toth G, Cober S G. 2007. Fog research: A review of past achievements and future perspectives. *Pure appl geophys*, 164: 1121–1159
- Guo L J, Guo X L, Fang C G, Zhu S C. 2015. Observation analysis on characteristics of formation, evolution and transition of a long-lasting severe fog and haze episode in North China. *Sci China Earth Sci*, 58: 329–344
- Haefelin M, Bergot T, Elias T, Tardif R, Carrer D, Chazette P, Colomb M, Drobinski P, Dupont E, Dupont J C, Gomes L, Musson-Genon L, Pietras C, Plana-Fattori A, Protat A, Rangognio J, Raut J C, Rémy S, Richard D, Sciare J, Zhang X. 2010. Parisfog. *Bull Amer Meteor Soc*, 91: 767–783
- Hong S Y, Noh Y, Dudhia J. 2006. A new vertical diffusion package with an explicit treatment of entrainment processes. *Mon Weather Rev*, 134: 2318–2341
- Jia X, Guo X. 2015. Impacts of secondary aerosols on a persistent fog event in Northern China. *Atmosph Ocean Sci Lett*, 5: 401–407
- Jiao S M, Zhu C Y, Zhu Y Y, Yuan C S, Zu F, Sun K Y. 2016. A discussion on the reason for a rare persistent heavy fog event in Jiangsu Province (in Chinese). *Acta Meteorol Sin*, 74: 202–212
- Jin G, Gao S, Shi H, Lu X, Yang Y, Zheng Q. 2022. Impacts of sea-land breeze circulation on the formation and development of coastal sea fog along the Shandong Peninsula: A case study. *Atmosphere*, 13: 165
- Jin W M, Wang X Y, Hong Z X, Zhao D S. 1983. Intermittent characteristics of ultra-low level jets under nighttime inversion conditions (in Chinese). *Atmos sci*, 7: 296–302
- Korb G, Zdunkowski W. 1970. Distribution of radiative energy in ground fog. *Tellus A-Dynam Meteor Oceanogr*, 22: 298–320
- Kunkel B. 1984. Parameterization of droplet terminal velocity and extinction coefficient in fog models. *J Appl Meteor*, 23: 34–41
- Li Z H, Huang J P, Sun B Y, Peng H. 1999. Burst characteristics during the development of radiation fog (in Chinese). *Atmos sci*, 23: 623–631
- Li Z H, Liu D Y, Yang J. 2011. The microphysical processes and macroscopic conditions of the radiation fog droplet spectrum broadening (in Chinese). *Atmos sci*, 35: 41–54
- Li Z, Liu D, Yan W, Wang H, Zhu C, Zhu Y, Zu F. 2019. Dense fog burst reinforcement over Eastern China: A review. *Atmos Res*, 230: 104639
- Liang M, Yang J, Wang W W, Yan W L, Pu M J. 2019. The burst reinforcement process of the twice heavy fog after the rain (in Chinese). *J Meteorol Sci*, 39: 153–163
- Liu Y L, Farley R D, Orville H D. 1983. Bulk parameterization of the snow field in a cloud model. *J Clim Appl Meteor*, 22: 1065–1092
- Liu D Y, Pu M J, Yang J, Zhang G Z, Li Z H. 2010. Microphysical structure and evolution of a four-day persistent fog event in Nanjing in December 2006. *Acta Meteorol Sin*, 24: 104–115
- Liu D, Yang J, Niu S, Li Z. 2011. On the evolution and structure of a radiation fog event in Nanjing. *Adv Atmos Sci*, 28: 223–237
- Liu D Y, Niu S J, Yang J, Zhao L J, Lv J J, Lu C S. 2012. Summary of a 4-year fog field study in northern Nanjing, Part I: Fog boundary layer. *Pure App Geophys*, 169: 809–819
- Liu D Y, Yan W L, Yang J, Pu M J, Niu S J, Li Z H. 2016. A study of the physical processes of an advection fog boundary layer. *Bound-Layer Meteorol*, 158: 125–138
- Liu D, Li Z, Yan W, Li Y. 2017. Advances in fog microphysics research in China. *Asia-Pac J Atmos Sci*, 53: 131–148
- Liu D Y, Yan W L, Qian J L, Liu M, Wang Z D, Cheng M N, Peng H Q. 2021. A movable fog-haze boundary layer conceptual model Over Jianghuai area, China. *Front Environm Sci*, 9: 823616
- Liu M, Yan W L, Zhang B, Yu J W, Jin X X. 2014. Analysis on persistence and intensification mechanism of fog and haze in Jiangsu in January 2013 (in Chinese). *Meteorol Month*, 40: 835–843
- Lu C S, Niu S J, Yang J, Liu X, Zhao L J. 2010. Jump features and causes of macro and microphysical structures of a winter fog in Nanjing (in Chinese). *Chin J Atmosph Sci*, 34: 681–690
- Lu X, Gao S H, Rao L J, Wang Y M. 2014. Sensitivity study of WRF parameterization schemes for the spring sea fog in the yellow sea (in Chinese). *J Meteorol Sci*, 25: 312–320
- Ma N, Zhao C S, Chen J, Xu W Y, Yan P, Zhou X J. 2014. A novel method for distinguishing fog and haze based on PM2.5, visibility, and relative humidity. *Sci China Earth Sci*, 57: 2156–2164
- Matsui T, Zhang S Q, Lang S E, Tao W K, Ichoku C, Peters-Lidard C D. 2020. Impact of radiation frequency, precipitation radiative forcing, and radiation column aggregation on convection-permitting West African Monsoon simulations. *Clim Dyn*, 55: 193–213
- Mlawer E J, Taubman S J, Brown P D, Iacono M J, Clough S A. 1997. Radiative transfer for inhomogeneous atmospheres: RRTM, a validated correlated-k model for the longwave. *J Geophys Res*, 102: 16663–16682
- Meyer M B, Jiusto J E, Lala G G. 1980. Measurements of visual range and radiation-fog (haze) microphysics. *J Atmos Sci*, 37: 622–629
- Mu M, Zhang R H. 2014. Addressing the issue of fog and haze: A promising perspective from meteorological science and technology. *Sci China Earth Sci*, 57: 1–2
- National Meteorological Centre. 2012. The Grade of fog forecast (GB/T 27964-2011) of the Compilation of Chinese National Standards. Beijing: Standards Press of China, 519
- Niu S, Lu C, Liu Y, Zhao L, Lü J, Yang J. 2010. Analysis of the microphysical structure of heavy fog using a droplet spectrometer: A case study. *Adv Atmos Sci*, 27: 1259–1275
- Niu S J, Liu D Y, Zhao L J, Lu C S, Lü J J, Yang J. 2012. Summary of a 4-year fog field study in northern Nanjing, Part 2: Fog microphysics. *Pure Appl Geophys*, 169: 1137–1155
- Taylor G I. 2007. The formation of fog and mist. *Quart J Royal Meteorol Soc*, 43: 241–268
- Okita T. 1962. Observations of the vertical structure of a stratus cloud and radiation fogs in relation to the mechanism of drizzle formation. *Tellus*, 14: 310–322
- Papanastasiou D K, Melas D, Bartanas T, Kittas C. 2010. Temperature, comfort and pollution levels during heat waves and the role of sea breeze. *Int J Biometeorol*, 54: 307–317
- Pilié R J, Mack E J, Rogers C W, Katz U, Kocmond W C. 1923. The Formation of marine fog and the development of fog-stratus systems

- along the California Coast. *J Appl Meteor*, 18: 1275–1286
- Price J. 2011. Radiation fog. Part I: Observations of stability and drop size distributions. *Bound-Layer Meteorol*, 139: 167–191
- Pu M J, Yan W L, Shang Z T, Yang Jun, Li Z H. 2008a. Study on the physical characteristics of burst reinforcement during the winter fog of Nanjing (in Chinese). *Plateau Meteorol*, 27: 1111–1118
- Pu M J, Zhang G Z, Yan W L, Li Z H. 2008b. Characteristics of a rare advection radiation fog process (in Chinese). *Sci Sinica Terra*, 38: 776–783
- Roach W T, Brown R, Caughey S J, Garland J A, Readings C J. 1976. The physics of radiation fog: I. A field study. *QJR Meteorol Soc*, 102: 313–333
- Shen P F, Liu D Y, Gultep I, Lin H J, Cai N H, Wang Z D. 2022. Boundary Layer Features of One Winter Fog in the Yangtze River Delta, China. *Pure and Applied Geophysics*
- Stull R B. 1988. An Introduction to Boundary Layer Meteorology. The Netherlands: Springer Dordrecht
- van der Velde I R, Steeneveld G J, Wicher Schreur B G J, Holtstag A A M. 2010. Modeling and forecasting the onset and duration of severe radiation fog under frost conditions. *Mon Weather Rev*, 138: 4237–4253
- Wang B H. 1980. The Continuation and dissipation of sea fog along China coast and its vicinity. *J Ocean Univ Qingdao*, 10: 20–30
- Wang B N, Zhang X R, Sun M, Tian L, Pu M J. 2020. Characteristics and formation mechanism of precipitation fog events in Jiangsu province (in Chinese). *J Meteorol Environ*, 36: 58–66
- Wang H B, Zhang Z W, Liu D Y, Yuan C S, Zhou L Y, Qian W. 2018. Detection of fog at night by using the new geostationary satellite Himawari-8 (in Chinese). *Plateau Meteorol*, 37: 1749–1764
- Wang H B, Wu H, Li Y, Xu J P, Zu F, Zhang Z W. 2020. Validation of rotorcraft UAV boundary layer meteorological observation data and its application in a heavy fog event in Yancheng (in Chinese). *Meteor Mon*, 46: 89–97
- Wang H B, Zhang Z W, Liu D Y, Zhu Y Y, Zhang X R, Yuan C S. 2020. Study on a large-scale persistent strong dense fog event in central and eastern China. *Adv Meteorol*, 2020: 8872334
- Wang H B, Zhang Z W, Liu D Y, Zu F, Zhu Y Y, Wu H. 2021. Characteristics of the macro-and micro-structures of the different grades fog in Jiangsu Province (in Chinese). *Plat Meteorol*, 40: 1177–1188
- Wang S, Fu D, Chen D L, Li P Y, Fu G. 2012. An observation and numerical simulation of a sea fog event over the Yellow Sea in the spring of 2009. *Trans Atmos Sci*, 35: 282–294
- Wang S Z, Song X L. 1989. The sea/land breeze in the northern coastal area of Shandong Peninsula. *Acta Oceanol Sin*, 8: 367–378
- Wang Y, Niu S, Lu C, Lv J, Zhang J, Zhang H, Zhang S, Shao N, Sun W, Jin Y, Song Q. 2021. Observational study of the physical and chemical characteristics of the winter radiation fog in the tropical rainforest in Xishuangbanna, China. *Sci China Earth Sci*, 64: 1982–1995
- Wei J S, Zhu W J, Yan W L, Sun Y, Wu J, Liu J W. 2010. Climatic characteristics of fog and its relevant influencing factors over the coastal areas of Jiangsu (in Chinese). *Trans Atmos Sci*, 33: 680–687
- Willett H C. 1928. Fog and haze, their causes, distribution, and forecasting. *Mon Wea Rev*, 56: 435–468
- Wu B G, Zhang H S, Zhang C C, Wang Z Y, Yu L L, Liu B X, Xie Y Y. 2008. Analysis of the micro-meteorologic element during the advection fog period in the south of Tianjin city (in Chinese). *Acta Scientiarum Naturalium Universitatis Pekinensis*, 44: 744–750
- Wu B G, Ma C P, Cai Z Y, Yu L, Zhao N, Qu X L. 2014. Mechanisms of local explosive development of a radiation fog event (in Chinese). *Plateau Meteorol*, 33: 1393–1402
- Wu D. 2008. Discussion on the distinction between haze and fog and analysis and processing of data (in Chinese). *Environ Chem*, 27: 327–330
- Xu H G, Deng B S, Zhou X G, Wang Q. 2002. Effect of fog on urban boundary layer and environment (in Chinese). *Chin J Atmosph Sci*, 13: 170–176
- Yan S Q, Zhu B, Huang Y, Zhu J, Kang H Q, Lu C S, Zhu T. 2020. To what extents do urbanization and air pollution affect fog? *Atmosph Chem Phys*, 20: 5559–5572
- Yan S, Zhu B, Zhu T, Shi C, Liu D, Kang H, Lu W, Lu C. 2021. The effect of aerosols on fog lifetime: Observational evidence and model simulations. *Geophys Res Lett*, 48: e2020GL61803
- Yan W L, Liu D Y, Pu M J, Li Z H. 2010. Formation and structure characteristics of precipitation fog in Nanjing (in Chinese). *Meteorol Mont*, 36: 29–36
- Yan W L, Zhu C Y, Zhu Y Y, Liu D Y, Pu M J. 2018. Study on a wide range of explosive heavy fog in Jiangsu (in Chinese). *Meteorol Mont*, 44: 892–901
- Yang J, Gao Y, Wu B G, Dong Q R, Wang Z Y, Hu H F. 2021. Advection fog process and its microphysical properties: A case study in Tianjin (in Chinese). *Trans Atmos Sci*, 44: 945–953
- Yin Z C, Wang H J, Guo W L. 2015. Climatic change features of fog and haze in winter over North China and Huang-Huai Area. *Sci China Earth Sci*, 58: 1370–1376
- Zhang G Z, Bian L G, Wang J Z, Yang Y Q, Yao W Q, Xu X D. 2005. Characteristics of boundary layer formed by fog in Beijing and its surrounding areas. *Sci China Ser D Earth Sci*, 35(Suppl): 73–83
- Zhang R, Li Q, Zhang R N. 2014. Meteorological conditions for the persistent severe fog and haze event over eastern China in January 2013. *Sci China Earth Sci*, 57: 26–35
- Zhou B B. 1994. On the relationship between fog and air pollution (in Chinese). *Meteorol Mont*, 20: 19–24
- Zhu C Y, Zhu Y Y, Zu F, Yan W L, Wang H B. 2018. Some Characteristics of the development of heavy fog in Autumn and Winter in Jiangsu Province (in Chinese). *Meteorol Mont*, 44: 1208–1219

(Editorial handling: Zhiyong MENG)